

Efficient Differentiable Causal Discovery via Reliable Super-Structure Learning

PINGCHUAN MA, Zhejiang University of Technology, China

QIXIN ZHANG, Nanyang Technological University, Singapore

SHUAI WANG, The Hong Kong University of Science and Technology, Hong Kong SAR

DACHENG TAO, Nanyang Technological University, Singapore

Recently, differentiable causal discovery has emerged as a promising approach to improve the accuracy and efficiency of existing methods. However, when applied to high-dimensional data or data with latent confounders, these methods, often based on off-the-shelf continuous optimization algorithms, struggle with the vast search space, the complexity of the objective function, and the nontrivial nature of graph-theoretical constraints. As a result, there has been a surge of interest in leveraging super-structures to guide the optimization process. Nonetheless, learning an appropriate super-structure at the right level of granularity, and doing so efficiently across various settings, presents significant challenges.

In this paper, we propose ALVGL, a novel and general enhancement to the differentiable causal discovery pipeline. ALVGL employs a sparse and low-rank decomposition to learn the precision matrix of the data. We design an ADMM procedure to optimize this decomposition, identifying components in the precision matrix that are most relevant to the underlying causal structure. These components are then combined to construct a super-structure that is provably a superset of the true causal graph. This super-structure is used to initialize a standard differentiable causal discovery method with a more focused search space, thereby improving both optimization efficiency and accuracy.

We demonstrate the versatility of ALVGL by instantiating it across a range of structural causal models, including both Gaussian and non-Gaussian settings, with and without unmeasured confounders. Extensive experiments on synthetic and real-world datasets show that ALVGL not only achieves state-of-the-art accuracy but also significantly improves optimization efficiency, making it a reliable and effective solution for differentiable causal discovery.

CCS Concepts: • **Mathematics of computing** → **Bayesian networks; Causal networks;** • **Computing methodologies** → *Causal reasoning and diagnostics*.

Additional Key Words and Phrases: causal discovery, Bayesian network

1 Introduction

Causal discovery is a fundamental problem in machine learning and statistics [30, 38], aiming to infer the underlying causal structure from observational data. It has wide-ranging applications across fields such as epidemiology, economics, and the social sciences. The task becomes especially challenging in high-dimensional settings or when latent confounders are present, prompting the development of a diverse set of methods, including constraint-based [11, 28, 30, 38], score-based [9, 10, 31, 32], and more recently, differentiable approaches [3, 4, 33, 39, 41].

Differentiable methods are particularly appealing because they reformulate causal discovery as a continuous optimization problem, enabling the use of gradient-based algorithms to learn causal structures directly from data. This is especially valuable in high-dimensional scenarios, where traditional methods often falter due to combinatorial explosion and computational bottlenecks. Despite their promise, differentiable approaches face significant challenges. Optimizing the entire graph structure, typically represented as a weighted adjacency matrix, is inherently difficult: the search space grows rapidly with dimensionality, and the presence of latent confounders further

Authors' Contact Information: Pingchuan Ma, pma@zjut.edu.cn, Zhejiang University of Technology, China; Qixin Zhang, Nanyang Technological University, Singapore; Shuai Wang, shuaiw@cse.ust.hk, The Hong Kong University of Science and Technology, Hong Kong SAR; Dacheng Tao, Nanyang Technological University, Singapore.

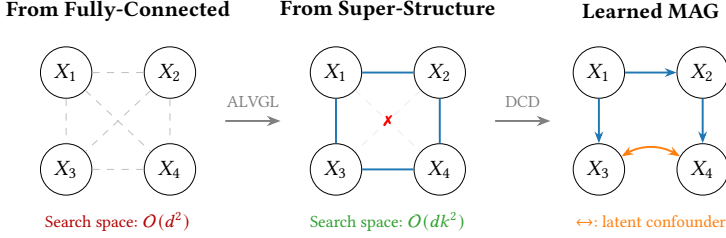


Fig. 1. Learning a MAG from a fully-connected graph vs. from a super-structure learned by ALVGL. DCD can be instantiated using any differentiable causal discovery method. Here, d is the number of variables and k is the maximum in-degree of the true causal graph.

complicates the objective landscape and constraints. As a result, existing methods often fail to converge to high-quality solutions within a reasonable timeframe and may end up with a cyclic graph, which is even not a valid causal structure.

Table 1. List of super-structure-guided optimizations.

	Type	Setting	Latent?	Super-structure
MMHC [31]	Score-based	Faithful	✗	Skeleton
CAM [7]	Score-based	Lin-Gauss	✗	Super Skeleton
GLasso [25]	Score-based	Lin-Gauss	✗	Moralized DAG
SPOT [20]	Differentiable	Lin-Gauss	✓	Skeleton
SDCD [23]	Differentiable	Faithful	✗	Preselected Edges
DCD w/ GLasso	Differentiable	Lin-Gauss	✗	Moralized DAG
DCD w/ ALVGL	Differentiable	Lin-Gauss	✓	Super Structure

Notably, these challenges are not exclusive to differentiable methods; score-based approaches, which rely on discrete optimization, face similar scalability issues. A widely adopted strategy in the score-based paradigm is to constrain the search space using a super-structure: a superset of the true causal graph that restricts the set of candidate edges [25, 31].

This idea has recently been extended to differentiable methods, where a super-structure is used to guide the optimization process [20, 23]. However, skeleton-based approaches such as SPOT typically incur high computational overhead due to the large number of conditional independence tests required, which limits their scalability in high-dimensional settings. In contrast, GLasso [25] provides a more efficient alternative by learning a moralized DAG using graphical Lasso, offering better scalability. Similarly, SDCD [23] selects edges via a constraint-free optimization process that, in the linear Gaussian setting, effectively reduces to graphical Lasso.

These observations prompt a natural question: *Can GLasso-style super-structure learning be combined with differentiable causal discovery (DCD) to yield a more efficient and effective optimization pipeline?* We explore this by applying GLasso as a pre-processing step for NOTEARS [41], and observe that, while incurring an 8.2% drop in F1 score, it achieves a substantial 78.7% reduction in runtime. Upon closer examination, the performance degradation is largely attributable to GLasso's inability to accurately estimate the precision matrix in high-dimensional regimes (e.g., $d \geq 100$). Moreover, real-world datasets often contain latent confounders, further diminishing its utility in guiding scalable differentiable causal discovery.

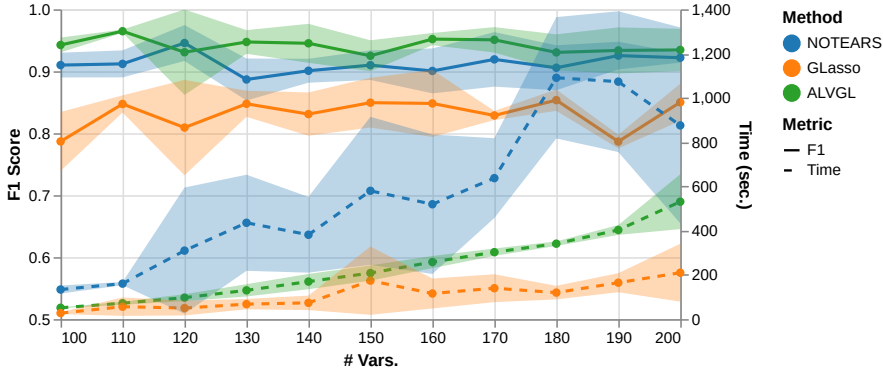


Fig. 2. Comparison of NOTEARS, GLasso and ALVGL on synthetic datasets ($n = 1000$, degree= 1, repeat three times).

These limitations lead us to a more ambitious question: *Can we design a super-structure learning method that remains robust in high-dimensional settings with latent confounders, while still being efficient enough to guide differentiable causal discovery?*

To address this, we propose ALVGL (Augmented Latent-Variable Graphical Lasso), a novel enhancement to differentiable causal discovery for linear Gaussian data, with or without latent confounders, by efficiently learning a super-structure to guide optimization and reduce the search space. ALVGL employs a sparse+low-rank decomposition of the precision matrix, inspired by the seminal framework of Chandrasekaran et al. [8], where the sparse component captures direct dependencies among observed variables and the low-rank component absorbs dense correlations from latent confounders or shared variance, ensuring robustness in high-dimensional settings unlike vanilla Graphical Lasso. To solve this decomposition efficiently, ALVGL employs an optimization strategy based on the Alternating Direction Method of Multipliers (ADMM), ensuring scalable and stable convergence even in high-dimensional scenarios. Finally, ALVGL introduces a robust super-structure learning method that combines information from sparse and low-rank components through a weighted adjacency matrix to accurately identify true causal connections while being aware of associations arising from latent confounding or limited sample sizes. Together, these optimizations enable ALVGL to consistently deliver accurate, efficient, and reliable super-structures for downstream differentiable causal discovery pipelines.

Evaluation Highlights. In Fig.2, we illustrate the performance advantages of ALVGL compared to NOTEARS [41] across multiple datasets. ALVGL consistently achieves significant improvements, boosting the F1 score by an average of 3.3% across all datasets while simultaneously reducing runtime by 52.9%. Notably, applying GLasso to these same datasets results in failure for 25 out of 33 scenarios due to ill-conditioned covariance matrices. Although the accuracy gain compared to NOTEARS appears modest, it is particularly noteworthy in the more challenging scenario involving latent confounders, where ALVGL boosts outperforms ABIC [4], improving F1 scores by 3.1% and runtime by 77.4%.

In summary, we make the following contributions:

- We propose a general framework for super-structure-guided differentiable causal discovery, which significantly improves scalability and reliability in challenging scenarios involving high-dimensional data and latent confounders.

- We introduce ALVGL, a new super-structure learning method, which decomposes the observed precision matrix into sparse and low-rank components. This allows it to robustly capture both direct dependencies and latent confounding effects while maintaining stability in high dimensions. We further show that the learned super-structure from ALVGL is theoretically guaranteed to contain the true causal graph and can be effectively integrated with a variety of existing differentiable causal discovery methods.
- Through extensive experiments on synthetic and real-world datasets, we demonstrate that ALVGL consistently improves both accuracy and efficiency, outperforming state-of-the-art baselines across a wide range of settings, especially in the presence of latent confounders.

Availability. We commit to open-sourcing ALVGL upon acceptance to foster transparency and facilitate further research.

2 Preliminary

In accordance with many previous works [4, 9, 10, 25, 32], we focus on discovering causal relationships of a linear Gaussian structural causal model (SCM) with or without latent confounders. In this section, we introduce the preliminary knowledge of SCM, differentiable causal discovery, and graphical Lasso.

2.1 Linear Gaussian SCM

Latent Confounder-Free SCM. We first start with the definition of a linear Gaussian SCM without latent confounders. Consider a linear SCM with d observable variables parameterized by a coefficient matrix $\delta \in \mathbb{R}^{d \times d}$. The SCM can be written as

$$X_i \leftarrow B_i^T X + N_i, \quad i = 1, \dots, d \quad (1)$$

where X_i is the i -th variable, B_i is a vector of coefficients for the parents of X_i in the DAG representation of the SCM, X is a vector of all variables, and N_i is a noise term that is mutually independent of all other noise terms. Specifically, a non-zero coefficient B_{ij} indicates that X_j is a parent of X_i in the DAG. (1) can be rewritten in matrix form as

$$X = B^T X + N \quad (2)$$

where $B = [B_1, \dots, B_d]$ corresponds to a weighted adjacency matrix of the DAG, $X = [X_1, \dots, X_d]^T$ is a vector of all variables, and $N = [N_1, \dots, N_d]$ is a vector of noise terms. The noise term N is characterized by a multi-variate Gaussian distribution with zero mean and covariance matrix $\Omega_N = \text{cov}(N) = \text{diag}(\sigma_1^2, \dots, \sigma_d^2)$, where σ_i^2 is the variance of the noise term N_i . We assume that $\sigma_i^2 > 0$ for all $i = 1, \dots, d$ to ensure positive measure everywhere. The covariance matrix Ω_X of the variables X can be expressed as $\Omega_X = (I - B)^{-T} \Omega_N (I - B)^{-1}$, where I is the identity matrix. The joint distribution of X is a zero-mean multivariate Gaussian distribution with covariance matrix Ω_X .

Latent Confounder SCM. When latent confounders are present, the linear SCM can be extended to include latent variables X_L . In this case, the latent variables can be encoded via the noise term N_i in (1), which is no longer mutually independent of other noise terms due to confounding effects. The covariance matrix Ω_N of the noise term N is no longer diagonal, and $\Omega_{N_{ij}} = \text{cov}(N_i, N_j)$ is non-zero if and only if X_i and X_j share a latent confounder. With this extension, the linear SCM on observable variables X_O can still be expressed in the similar form as

$$X_O = B^T X_O + N \quad (3)$$

And, likewise, the covariance matrix of the observable variables X_O can be expressed as $\Omega_{X_O} = (I - B)^{-T} \Omega_N (I - B)^{-1}$.

Graphical Representation. The SCM defined above can be represented as a causal graph $G = (V, E)$, where $V = \{V_1, \dots, V_d\}$ is a set of nodes representing the variables X (or, in the case of latent confounders, X_O), and E is a set of directed (and bidirected, if latent confounders are present) edges representing the causal relationships between the variables. Under the *structural minimality* assumption [26], one can derive the causal graph from the linear SCM with the following rules: (1) if $B_{ij} \neq 0$, then there is a directed edge $V_i \rightarrow V_j$ in the graph; (2) if latent confounders are present, then there is a bidirected edge $V_i \leftrightarrow V_j$ if $\Omega_{N_{ij}} \neq 0$. Thus, the goal of causal discovery recasts to inferring B and Ω_N from the empirical observations of X (or X_O).

2.2 Differentiable Causal Discovery

Score-based methods aim to maximize a score function (e.g., log-likelihood) over graph structures, subject to the acyclicity constraint. This can be formulated as:

$$\arg \max_G f(G) \text{ s.t. } G \text{ is acyclic} \quad (4)$$

where $f(\cdot)$ is the score function. Due to the acyclicity constraint, this optimization is inherently combinatorial. Recently, differentiable approaches have relaxed this problem by reformulating the acyclicity constraint into a continuous function — most notably:

$$h_{\text{DAG}}(B) = \text{tr}(e^{B \circ B}) - d \quad (5)$$

where $d = |\mathcal{V}_O|$ is the number of observed variables, and B is the weighted adjacency matrix of the graph G , as defined in Sec. 2.1. This function satisfies $h_{\text{DAG}}(B) = 0$ if and only if G is acyclic. Several variants of h_{DAG} have been proposed to improve numerical stability and computational efficiency [3, 34, 36, 40, 42]. Typically, these formulations are optimized using augmented Lagrangian methods (ALM) or the alternating direction method of multipliers (ADMM), which decompose the constrained problem into a series of unconstrained subproblems solvable via standard optimizers.

Despite these advances, the optimization remains challenging. The objective function is often complex, and the acyclicity constraint h_{DAG} introduces significant non-convexity. In particular, B scales quadratically with the number of variables, and the constraint h_{DAG} has at least polynomial degree in B , depending on its specific form. Consequently, differentiable methods often struggle to converge to meaningful solutions in large-scale settings.

The scalability issues are exacerbated when latent confounders are present, as both the objective function and the constraints become more complex. As aforementioned, the causal graph G requires both B and Ω_N to represent the directed and bidirected edges, respectively. Since bidirected edges are introduced, the graph is represented as an ancestral directed mixed graph (ADMG) [27]. The corresponding structural constraint for ADMGs [4] can be expressed as

$$h_{\text{ADMG}}(B, \Omega_N) = \text{tr}(e^B) - d + \text{sum}(e^B \circ \Omega_N) \quad (6)$$

The function h_{ADMG} is a generalization of h_{DAG} to accommodate the bidirected edges in ADMGs. It has been proved that $h_{\text{ADMG}}(B, \Omega_N) = 0$ if and only if G is an ancestral ADMG. And, additional complexity is also introduced in the objective function for differentiable ADMG learning. We omit the details of the objective function here as it is independent of our interests in this paper, and refer readers to the original paper [4].

2.3 Graphical Lasso

Graphical Lasso [14] is a widely used method for estimating the precision matrix (the inverse of the covariance matrix) of a multivariate Gaussian distribution. We state the problem as follows. Consider a set of variables $X = [X_1, \dots, X_d]^T$ from a zero-mean multivariate Gaussian distribution

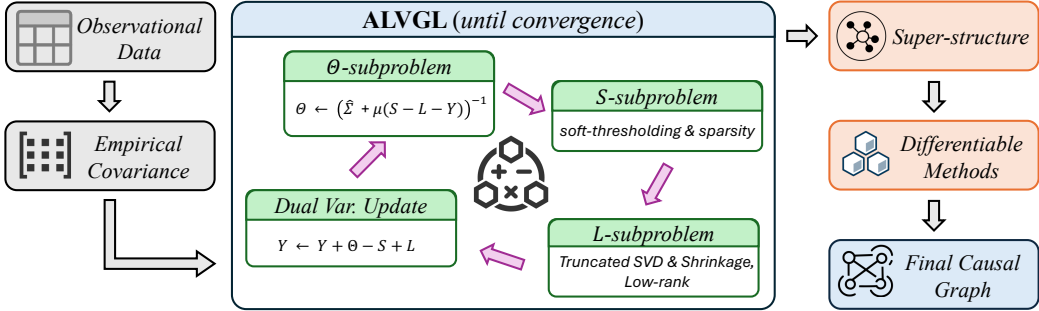


Fig. 3. Overview

with a covariance matrix $\Omega_X = \text{cov}(X)$. The graphical Lasso aims to estimate the precision matrix Θ which is the inverse of covariance matrix Ω_X^{-1} by solving the following optimization problem:

$$\arg \min_{\Theta \succeq 0} -\log \det(\Theta) + \text{tr}(\Omega_X \Theta) + \lambda \|\Theta\|_1 \quad (7)$$

where λ is a regularization parameter that controls the sparsity of the estimated precision matrix. The first two terms in the objective function are the negative log-likelihood of the Gaussian distribution, and the third term is an ℓ_1 -norm regularization term that encourages sparsity in the precision matrix Θ . An important property of the precision matrix is that if $\Theta_{ij} = 0$ and X is linear Gaussian, then X_i and X_j are conditionally independent given all other variables, i.e., $X \setminus \{X_i, X_j\}$. The undirected graph corresponding to the precision matrix Θ is known as the *conditional independence graph* [18], which is the *moralized DAG* for the setting without latent confounders. Since the *moralized DAG* is a super graph of the true causal graph, graphical Lasso can be used as a prescreening step to reduce the search space for causal discovery methods [7, 18, 25].

While graphical lasso has proven effective in many applications, it faces several limitations when applied to high-dimensional data and complex dependency structures. First, the method assumes that all conditional dependencies can be captured through direct pairwise relationships in the precision matrix, failing to account for *latent confounders* that may induce spurious correlations between observed variables [8]. Second, graphical lasso relies on a SPD covariance matrix Ω_X to ensure the resulting optimization problem is well-posed. However, under high-dimensional settings where the sample size n is not significantly larger than the number of variables d (i.e., $n \not\gg d$), or when the underlying graph has dense structures or subtle noises (i.e., nearly linearly dependent variables), the resulting matrix may become rank-deficient during optimizations, leading to ill-conditioned problems.

3 ALVGL

Inspired by the success of super-structure-guided optimization in score-based methods, we are motivated to improve the limitations of graphical Lasso and learn a super-structure that can better guide the optimization of differentiable causal discovery methods. We start with formulating the problem setting and then present our approach.

3.1 Problem Setting

We consider the task of causal structure discovery in the presence of latent confounders under the linear Gaussian assumption. Let $X_O = [X_1, \dots, X_d]^T \in \mathbb{R}^{d \times n}$ denote a dataset of d observed variables with n samples, where each X_i is a real-valued random variable, and the observations

are generated from a linear Gaussian SCM that may include latent variables. The goal is to learn a *super-structure* – an undirected graph over X_O that contains all true edges of the underlying causal graph – to restrict and guide the search space for downstream causal discovery algorithms.

We assume the data follows a linear SCM with additive Gaussian noise:

$$\mathbf{X} = \mathbf{B}^T \mathbf{X} + \mathbf{N} \quad (8)$$

where $\mathbf{X} \in \mathbb{R}^{(d+\ell) \times n}$ consists of both observed variables X_O and latent variables X_L , \mathbf{B} is a coefficient matrix encoding the causal relationships (possibly including connections to latent variables), and $\mathbf{N} \sim \mathcal{N}(0, \Omega_N)$ is a zero-mean Gaussian noise vector. We let $\Sigma_O = \text{cov}(X_O)$ denote the marginal covariance matrix over observed variables, and our aim is to recover structural information about the true causal graph using only access to X_O . Specifically, when $l = 0$, the true causal graph is a DAG over X_O ; when $l > 0$, the true causal graph is a maximal ancestral graph (MAG) over X_O that may include both directed and bidirected edges due to latent confounding [27].

In the following, we make the standard assumptions commonly adopted in the causal discovery literature [4, 26] and forms the basis of our theoretical analysis.

- (A1) **Linear Gaussian SCM with latent variables.** The joint distribution of (X_O, X_L) is generated by a linear Gaussian SCM of the form above whose causal structure is represented by a directed acyclic graph (DAG) over observed and latent variables, possibly inducing a mixed graph over X_O after marginalizing out latents.
- (A2) **Faithfulness and structural minimality.** The joint distribution is faithful and structurally minimal with respect to the underlying causal graph [26]. In particular, for DAGs and mixed graphs, missing edges (or graphical separations in general) correspond to conditional independencies, and there is no exact cancellation of parameters that would mask an existing edge (i.e., by manifesting a detectable statistical dependence *w.r.t* a threshold τ).

3.2 On the Implication of Latent Variables

A major challenge in causal discovery with latent variables is that marginalizing out these unobserved variables distorts the conditional independence structure among the observed ones. In particular, the marginal precision matrix $\Theta_O = \Sigma_O^{-1}$, where Σ_O is the covariance matrix over the observed variables X_O , no longer reflects a sparse structure, even when the true causal graph is sparse. This violates the core assumption of methods like graphical Lasso, which rely on the sparsity of Θ_O to recover meaningful structural information.

To understand the issue, we distinguish between two ways of interpreting the precision matrix. On one hand, Θ_O encodes the conditional independencies among observed variables given only other observed variables, since it is computed as the inverse of the marginal covariance Σ_O . On the other hand, the correct conditional independence structure that aligns with the full causal model, including latent variables, is represented by the submatrix $\tilde{\Theta}_O = \Theta_{O+L}[O, O]$ of the full precision matrix $\Theta_{O+L} = \Sigma_{O+L}^{-1}$. In this case, $\tilde{\Theta}_O$ reflects conditional independencies among observables given all remaining observed and latent variables. The two matrices differ: while $\Theta_{O_{ij}} = 0$ implies X_i and X_j are independent conditioned only on other observables, $\tilde{\Theta}_{O_{ij}} = 0$ implies independence even after accounting for latent confounding.

In the context of causal discovery, one might hope that Θ_O is sufficient to determine the super-structure, since an edge in the true causal graph implies that X_i and X_j are not conditionally independent given any subset of the other observed variables. This would suggest that directly applying graphical Lasso to estimate Θ_O from Σ_O could suffice. However, this intuition is misleading. Marginalizing over latent variables causes their influence to spread across the observed space, and the resulting precision matrix Θ_O becomes dense, with indirect effects falsely appearing as direct

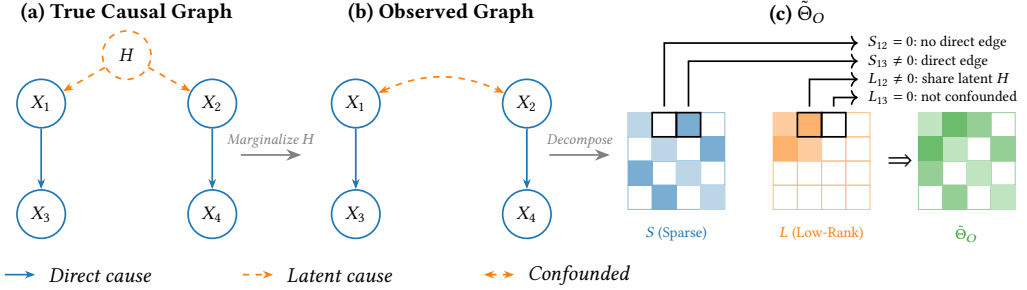


Fig. 4. Illustration of sparse+low-rank decomposition. (a) The true causal graph includes a latent confounder H affecting X_1 and X_2 , with direct edges $X_1 \rightarrow X_3$ and $X_2 \rightarrow X_4$. (b) After marginalizing H , its effect appears as a bidirected edge $X_1 \leftrightarrow X_2$. (c) The precision matrix $\tilde{\Theta}_O$ decomposes into sparse S and low-rank L . $S_{ij} \neq 0$ indicates a direct causal relationship between X_i and X_j ; $L_{ij} \neq 0$ indicates that X_i and X_j are jointly influenced by shared latent variables; $\tilde{\Theta}_{O,ij}$ combines both effects to represent the full conditional dependency structure.

ones. The sparsity assumption on Θ_O no longer holds, making graphical Lasso inapplicable in this setting [8]. Therefore, it is crucial to account for latent confounding explicitly when estimating the precision matrix. A better alternative is to model the observed conditional independencies via a decomposition of the full precision structure into a sparse component, capturing direct effects among observables, and a low-rank component, capturing dependencies induced by latent variables. We turn to this approach in the next section.

3.3 Sparse+Low-Rank Decomposition

Fig. 4 provides an intuitive illustration of how a precision matrix with latent confounding effects naturally separates into a *sparse* component S capturing direct causal relationships among observed variables and a *low-rank* component L capturing shared variation induced by latent factors. Panel (a) shows the true causal graph with a latent variable H influencing X_1 and X_2 . After marginalizing H , its effect appears in panel (b) as a bidirectional edge $X_1 \leftrightarrow X_2$, which is a hallmark of latent confounding. Panel (c) then visualizes the decomposition $\tilde{\Theta}_O = S - L$, where annotated matrix cells illustrate that nonzero entries in S (blue blocks) correspond to direct causal relations (e.g., $S_{13} \neq 0$), while nonzero entries in L (orange blocks) correspond to latent-induced correlations (e.g., $L_{12} \neq 0$ because X_1 and X_2 share H), and the final precision $\tilde{\Theta}_O$ reflects their combined effects.

Recall that the observed precision matrix $\tilde{\Theta}_O$ consists of ① Θ_O , the conditional dependencies among observed variables, and ② a low-rank component encoding the conditional dependencies induced by latent variables. Formally, following Chandrasekaran et al. [8], the precision matrix after marginalizing latent variables can be expressed via the Schur complement as:

$$\tilde{\Theta}_O = \underbrace{\Theta_O}_{S} - \underbrace{\Theta_{OL}\Theta_L^{-1}\Theta_{LO}}_{L}, \quad (9)$$

where Θ_{OL} is the cross-precision between observed and latent variables, and Θ_L is the precision of the latent variables.

Connection to Fig. 4. In panel (a), the latent variable H induces correlations among X_1 and X_2 . This translates algebraically into the low-rank term $L = \Theta_{OL}\Theta_L^{-1}\Theta_{LO}$ in (9), which appears in panel (c) as highlighted orange cells such as $L_{12} \neq 0$. Conversely, direct causal edges such as $X_1 \rightarrow X_3$ manifest

as nonzero entries in S , e.g., $S_{13} \neq 0$ (blue cells). The decomposition thus separates the effects of direct causation and latent confounding into interpretable structural components.

To estimate the decomposition, Chandrasekaran et al. [8] proposed the convex program:

$$\begin{aligned} \min_{S-L \succ 0, L \succeq 0} \mathcal{L}(S, L) = & -\log \det(S - L) + \text{tr}[(S - L)\hat{\Sigma}] \\ & + \lambda_s \|S\|_1 + \lambda_l \|L\|_*, \end{aligned} \quad (10)$$

where $\|S\|_1$ enforces sparsity to recover direct dependencies (blue blocks in panel (c)), and $\|L\|_*$, the nuclear norm, enforces low-rank structure matching the shared latent effects (orange blocks in panel (c)). The resulting estimate of Θ_O is thus recovered as S , while L provides an interpretable summary of latent confounding patterns. As shown in panel (c), S and L jointly reconstruct $\tilde{\Theta}_O$ (green matrix), demonstrating how direct and latent-induced dependencies combine.

When no latent confounders exist, L is expected to be zero and $\tilde{\Theta}_O = \Theta_O$. Even in this setting, the sparse+low-rank model is empirically more robust than graphical Lasso, particularly when n is not significantly larger than d . The low-rank component naturally absorbs dense, spurious correlations caused by small sample sizes or model misspecification, preventing contamination of the sparse structure in S . This leads to improved conditioning and more stable convergence of the precision estimation problem.

3.4 ADMM Optimization

To solve the optimization problem stated in (10), we first present a reformulation of the problem that allows us to use the Alternating Direction Method of Multipliers (ADMM) [5]. We introduce an auxiliary variable $\Theta = S - L$, which leads to the following equivalent formulation:

$$\min_{\Theta \succ 0, L \succeq 0, S} -\log \det(\Theta) + \text{tr}(\Theta\hat{\Sigma}) + \lambda_s \|S\|_1 + \lambda_l \|L\|_* \quad (11)$$

$$\text{subject to } \Theta = S - L \quad (12)$$

The equality constraint $\Theta = S - L$ is where ADMM comes in. We have the following augmented Lagrangian function:

$$\mathcal{L}_\mu(\Theta, S, L, Y) = -\log \det(\Theta) + \text{tr}(\Theta\hat{\Sigma}) + \lambda_s \|S\|_1 \quad (13)$$

$$+ \lambda_l \|L\|_* + \frac{\mu}{2} \|\Theta - S + L + Y\|_F^2. \quad (14)$$

where the residual $R := \Theta - (S - L)$ is captured by the dual variable Y . We have the subproblem updates as follows

$$\begin{aligned} \Theta^{k+1} &= \arg \min_{\Theta \succ 0} -\log \det \Theta + \text{tr}(\Theta\hat{\Sigma}) + \frac{\mu}{2} \|\Theta - S^k + L^k + Y^k\|_F^2, \\ S^{k+1} &= \arg \min_S \lambda_s \|S\|_1 + \frac{\mu}{2} \|\Theta^{k+1} - S + L^k + Y^k\|_F^2, \\ L^{k+1} &= \arg \min_{L \succeq 0} \lambda_l \|L\|_* + \frac{\mu}{2} \|\Theta^{k+1} - S^{k+1} + L + Y^k\|_F^2, \\ Y^{k+1} &= Y^k + \Theta^{k+1} - S^{k+1} + L^{k+1}. \end{aligned} \quad (15)$$

By solving these subproblems iteratively, we can obtain the estimates of S and L . We present the operational procedure in Alg. 1.

In line 1, Alg. 1 initializes the sparse matrix S as the inverse of the empirical covariance $\hat{\Sigma}$ (or a regularized version if $\hat{\Sigma}$ is singular), the low-rank matrix L and the scaled dual variable Y as zero matrices, and the penalty parameter μ to an initial value. It then proceeds through a series of iterative updates for Θ , S , L , and Y :

Algorithm 1: ALVGL-ADMM

Input: $\hat{\Sigma}$: empirical covariance; λ_s, λ_l : regularization; τ : threshold; T : max iterations

- 1 Initialize $(S, L, Y, \mu) \leftarrow (\hat{\Sigma}^{-1}, 0, 0, 1)$;
- 2 **for** $t = 1, \dots, T$ **or until converged do**
- 3 $\Theta \leftarrow \left(\hat{\Sigma} + \mu(S - L - Y) \right)^{-1}$; *// solve Θ -subproblem*
- 4 $S \leftarrow \text{soft}_{\frac{\lambda_s}{\mu}}(\Theta + L + Y)$; *// solve S -subproblem*
- 5 $\lambda_{\max} \leftarrow \max(\text{eig}(\hat{\Sigma}))$;
- 6 $r^* \leftarrow \sum_{i=1}^d \mathbb{I}(\lambda_i > \tau \cdot \lambda_{\max})$;
- 7 $[U, s, V^T] \leftarrow \text{SVD}(\Theta - S + Y)$;
- 8 $s \leftarrow \text{shrink}(s, \frac{\lambda_l}{\mu}, r^*)$;
- 9 $L \leftarrow U \cdot \text{diag}(s) \cdot V^T$; *// solve L -subproblem*
- 10 $Y \leftarrow Y + \Theta - S + L$; *// dual variable update*
- 11 Update μ ;
- 12 **end**
- 13 **return** S, L

- (1) **Θ -update (line 3):** The precision matrix Θ^{k+1} is updated by computing the inverse of the effective covariance matrix $(\hat{\Sigma} + \mu^{(k)}(L^{(k)} - Y^{(k)}))$, which is an inexact yet computationally cheap ADMM update.
- (2) **S -update (line 4):** The sparse component S is updated to encourage sparsity while fitting the data, which is done by applying the element-wise soft-thresholding operator soft_α to $\Theta^{(k+1)}$. Here, soft_α is defined as:

$$\text{soft}_\alpha(S)_{ij} = \text{sign}(S_{ij}) \max(|S_{ij}| - \alpha, 0) \quad (16)$$

This operation shrinks the elements of $\Theta^{(k+1)}$ towards zero, promoting sparsity in the resulting matrix $S^{(k+1)}$. The threshold α is set to $\frac{\lambda_s}{\mu^{(k)}}$, where λ_s is the regularization parameter for sparsity and $\mu^{(k)}$ is the penalty parameter at iteration k .

- (3) **L -update (line 5–9):** The textbook ADMM step for the L -update requires a full SVD of the residual matrix with soft-thresholding to ensure positive semidefiniteness. Recall that L is expected to be low-rank in the problem setting, so we pre-estimate a plausible latent dimension $r^* \ll d$ and apply a shrink operator to implement truncated singular value thresholding where only the top r^* singular values are retained.¹ Finally, we reconstruct the low-rank component $L^{(k+1)}$ using the truncated singular values such that the positive semidefiniteness is enforced. Compared to the exact solution, this approximation is computationally efficient and numerically more robust.
- (4) **Y -update (line 10):** The scaled dual variable Y is updated using the residual and enforces the equality constraint $\Theta = S - L$ over the iterations.

These steps are repeated until a convergence criterion is met, or a maximum number of iterations T is reached. The algorithm then returns the estimated S and L .

Remark. *Despite several approximations are introduced in the ADMM updates, by the inexact ADMM theory [5, 12], Alg. 1 can still converge under some mild conditions. Empirically, we find it works better on our task compared to the standard ADMM-based latent-variable graphical Lasso algorithm [21].*

¹Computing r^* is an one-time effort and we place it inside the loop for better readability.

ALVGL vs. Classical LVGL. Unlike LVGL [8], which optimizes the decomposition exclusively for precision estimation, ALVGL modifies both the penalty structure and the decomposition objective to maximize support recovery quality of S for super-structure construction. This design avoids the common leakage of true edges into the low-rank component, a failure mode that severely limits LVGL when used for structural tasks, as we will demonstrate in Sec. 4.2.

3.5 Super-Structure Learning

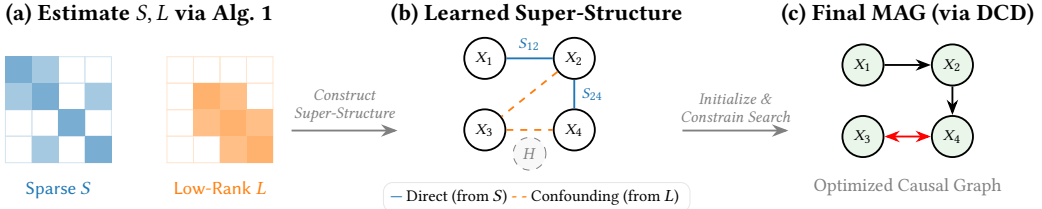


Fig. 5. Workflow of ALVGL. (a) The precision matrix Θ is decomposed into Sparse (S) and Low-Rank (L) components. (b) These components are combined to form a Super-Structure containing both direct and latent associations. (c) This structure constrains the search space for Differentiable Causal Discovery (DCD) to efficiently output the final causal graph (MAG in this case).

In general, one might expect that the sparse component S (i.e., Θ_O in (9)) alone would suffice to derive the desired super-structure, because $\Theta_{O_{ij}} = 0$ implies X_i and X_j are conditionally independent given all other observed and latent variables. However, this implication highlights a critical caveat: in the presence of latent confounders, $\Theta_{O_{ij}} = 0$ does not guarantee that X_i and X_j are conditionally independent given only the other observed variables. Instead, conditional independence is only assured when conditioning on all other variables (both observed and latent). As a direct consequence, relying solely on S may fail to recover all edges present in the true causal graph in the sense that missing links may arise wherever latent confounding obscures conditional dependencies among observables. Even if latent variables are absent, incorporating information from the low-rank component L can still improve super-structure learning. This is because L not only captures shared variation induced by latent confounders in an asymptotic regime, but also helps absorb dense or spurious correlations from finite data samples or model misspecification in practical settings, thereby enhancing robustness and stability in estimation.

To further clarify, as schematically illustrated in Fig. 5, our approach computes the combined adjacency matrix from both components (Fig. 5 (a)):

$$W = |S| + |L| \quad (17)$$

The resulting super-structure (Fig. 5 (b)) is then obtained by thresholding the combined adjacency matrix $G^* = \mathbb{I}[W > \tau]$.

Remark. In (9), the low-rank component L is subtracted from the sparse component S to yield the precision matrix $\tilde{\Theta}_O$, consistent with the decomposition of latent-variable graphical models. However, in (17), we instead combine S and L additively to construct the combined adjacency matrix W . This shift reflects a change in objective: while the decomposition aims to model conditional independencies, super-structure learning seeks to robustly identify potential (either direct or confounded) edges. As an analogy to FCI [38], L can be viewed as capturing strong marginal associations that manifest as bidirected edges in the underlying mixed graph. By combining both components, our super-structure G^* conservatively includes all plausible causal and confounded links, ensuring no true edge is pruned

prematurely. This strategy aligns with the goal of constructing a reliable (yet not necessarily minimal) super-graph of the causal structure.

Hypergraph Interpretation. Because L captures shared confounding patterns that typically manifest as bidirected edges in ADMGs, ALVGL’s combined adjacency W implicitly encodes a hypergraph over observed variables. This provides structural information that LVGL [8] usually discards, and is crucial for ensuring that no true causal relation is eliminated during thresholding.

The following proposition states that the super-structure learned by ALVGL is a valid super structure, i.e., it contains all the edges in the true causal graph, and thus can be used to guide the differentiable optimization process of existing differentiable causal discovery methods (Fig. 5 (c)).

PROPOSITION 3.1. *Let G^* be the super-structure learned by ALVGL, and let G^* be the true causal graph. Under assumptions A1–A2, G^* is a super structure of G^* , i.e., $G^* \supseteq G^*$, with or without latent confounders.*

PROOF. We prove that the super-structure G^* learned by ALVGL contains all edges of the true causal graph G^* , regardless of the presence of latent confounders. For both DAGs and MAGs, under the linear Gaussian assumption (A1) and faithfulness (A2), any edge $\{i, j\} \in G^*$ implies that $X_i \not\perp\!\!\!\perp X_j \mid X_O \setminus \{X_i, X_j\}$, meaning $\Theta_{O,ij} \neq 0$, where $\Theta_O = S$. Under the identifiability conditions [8], the estimator (10) can recover the support of S , so with high probability (w.h.p.), $|S_{ij}| + |L_{ij}| > \tau$ for all true edges, provided τ is chosen appropriately (e.g., $\tau = 0$ for a conservative estimate). Since $W = |S| + |L|$ is used to construct $G^* = \mathbb{I}[W > \tau]$, this guarantees $G^* \supseteq G^*$ w.h.p. Thus, G^* is a valid super-structure of G^* . \square

In the absence of latent confounders, the super-structure learned by ALVGL can be characterized as a moralized DAG of the true causal graph, with the following proposition stating the property.

PROPOSITION 3.2. *Let G^* be the super-structure learned by ALVGL, and let G^* be the true causal graph. If there are no latent confounders and the assumptions of Proposition 3.1 hold, then G^* is a moralized DAG of G^* .*

PROOF SKETCH. When there are no latent confounders, the low-rank component L is zero and Θ_O is equal to $\tilde{\Theta}_O$. Then, the above proposition is a direct consequence of Theorem 1 in [25]. \square

COROLLARY 3.3. *With Proposition 3.2 and Lemma A.3 of [23], if G^* has maximal in-degree of k and let d be the number of observed variables, then G^* has at most $O(dk^2)$ edges, which is usually much smaller than the $O(d^2)$ edges in a full adjacency matrix.*

3.6 Computational Complexity

For each ADMM iteration, the dominant costs are a matrix inversion ($O(d^3)$) and an SVD with rank truncation. This is $O(d^3)$ in the worst case, but can be reduced to $O(d^2r^*)$ using economy decomposition, where d is the number of observed variables and r^* is the effective rank of the low-rank component L . The method usually takes a small fraction of the entire runtime of differentiable causal discovery methods, while providing a significant boost in optimization efficiency, as will be shown in Sec. 4.

3.7 Integration in Differentiable Optimization

ALVGL outputs a binary super-structure mask $G^* \in \{0, 1\}^{d \times d}$ encoding the set of edges that are allowed to be nonzero. Let $\mathcal{Z} = \{(i, j) \mid G_{ij}^* = 0\}$ denote the forbidden edges. A differentiable causal discovery method solves

$$\min_{W \in \mathbb{R}^{d \times d}} \mathcal{J}(W) \quad \text{s.t.} \quad h(W) = 0, \quad (18)$$

where $h(W)$ enforces acyclicity or other structural constraints. Incorporating the ALVGL super-structure introduces additional linear equality constraints

$$W_{ij} = 0 \quad \text{for all } (i, j) \in \mathcal{Z}, \quad (19)$$

which restrict the feasible set to the linear subspace

$$\mathcal{W}_{G^*} := \{ W \in \mathbb{R}^{d \times d} : W \circ (1 - G^*) = 0 \}, \quad (20)$$

reducing the intrinsic optimization dimension from d^2 parameters to $\|G^*\|_0$. By Proposition 3.1, ALVGL recovers a valid super-structure *w.h.p.*, meaning every true edge (i, j) satisfies $G_{ij}^* = 1$. Thus, if W^* denotes the true weighted adjacency matrix, $W^* \in \mathcal{W}_M$, and the following solution-preservation result holds.

PROPOSITION 3.4 (SOLUTION PRESERVATION). *If G^* is a valid super-structure for the true solution W^* (i.e., $G_{ij}^* = 0 \implies W_{ij}^* = 0$), then any global minimizer of the full problem remains a global minimizer of the restricted problem*

$$\min_{W \in \mathcal{W}_{G^*}} \mathcal{J}(W) \quad \text{s.t.} \quad h(W) = 0. \quad (21)$$

This implies that restricting the domain does not eliminate valid solutions. Instead, it removes an exponentially large portion of structurally impossible configurations. In convex analogues, projecting onto such a constraint subspace both preserves the optimum and can *improve conditioning* by eliminating noisy gradient directions, yielding faster convergence. While $h(W)$ introduces non-convexity, empirical results in Sec.4 show that the same benefits manifest in practice: faster convergence, more stable L-BFGS updates, and large runtime reductions in high-dimensional regimes.

Implementation via projected gradients. During optimization, we maintain $W^{(0)} \in \mathcal{W}_M$ and update only free parameters. At iteration k , if $G^{(k)} = \nabla \mathcal{J}(W^{(k)})$ is the gradient, the projected update is

$$G_{\text{proj}}^{(k)} = G^{(k)} \circ M, \quad (22)$$

ensuring forbidden edges never change. Similarly, any second-order information is projected to \mathcal{W}_{G^*} as well. The L-BFGS solver (or any gradient-based optimizer) then operates entirely within \mathcal{W}_{G^*} . This direct enforcement of hard constraints differs from soft mask regularization approaches, which merely discourage unwanted edges. Because ALVGL achieves consistently high recall, the risk of excluding true edges is negligible, making hard constraints both safe and far more computationally effective. This principle is also adopted in recent causal discovery methods [20, 23].

4 Evaluation

In evaluation, we aim to evaluate the performance of ALVGL from three perspectives: ① universal enhancement to diverse differentiable causal discovery methods; ② comparison with other super-structure learning methods; ③ robustness to diverse settings and misspecified data and ④ a case study on real-world datasets.

Data Generation. Our experiments involve two settings, including linear Gaussian SCMs with latent confounders and linear Gaussian SCMs without latent confounders. For the first setting, we follow the same parametric setup as ABIC [4] and SPOT [20] and generate ADMGs with 15–25 nodes and 1000 samples. For the second setting, we follow the same parametric setup as NOTEARS [41] and generate DAGs with 100–200 nodes and 1000 samples. For each setting, we generate datasets with Erdos-Renyi (ER) graphs with a fixed degree of 1 in main comparison. We also explore the

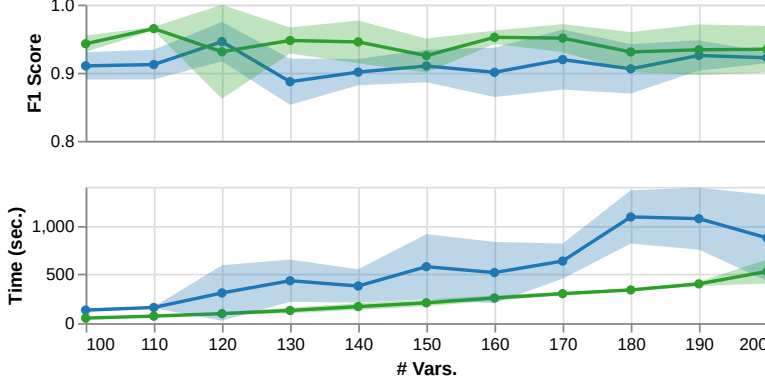


Fig. 6. NOTEARS vs. NOTEARS*.

effectiveness of ALVGL on larger graphs, different graph structures, including scale-free (SF) graphs and bipartite (BP) graphs, degrees and sample sizes in Sec. 4.3.

Baselines. We implement ALVGL on four representative differentiable causal discovery methods: NOTEARS [41] (2018), GOLEM [24] (2020), DAGMA [3] (2022), and ABIC [4] (2021). The first three methods are designed for linear Gaussian data without latent confounders, while ABIC is designed for linear Gaussian data with latent confounders. We denote the resulting methods as NOTEARS*, GOLEM*, DAGMA*, and ABIC*, respectively.

In addition, we implement graphical lasso (GLasso) [14], latent variable graphical lasso (LVGL) [8], and skeleton learning [20] as alternative super structure learning methods. These super structures replicate the functionality of SDCD [23] (2024), ALVGL’s ablation without the optimizations described in Sec. 3, and SPOT [20] (2024), respectively. We denote these methods as GLasso, LVGL, and SL, and use NOTEARS as the base differentiable causal discovery method.

All baselines use the default hyperparameters suggested in their documentation. For ALVGL, we set the hyperparameters $\lambda_s = 0.05$, $\lambda_l = 0.05$, $\tau = 1 \times 10^{-6}$, and $T = 500$ for all experiments.

4.1 End-to-end Comparison

NOTEARS. Fig. 6 shows that NOTEARS* consistently outperforms NOTEARS on synthetic datasets, achieving an average F1 improvement of 3.3%. Runtime is reduced by 52.9%, and importantly, variance in runtime is also substantially lower (29.30 vs. 233.09). This reflects the stabilizing effect of ALVGL, which constrains the search space via learned super-structures. Furthermore, NOTEARS* scales more gracefully with graph size, which validates Corollary 3.3, as its search space does not grow quadratically like NOTEARS.

GOLEM and DAGMA. Fig. 7 compares GOLEM and DAGMA with their * counterparts. We report only F1 scores due to fixed iteration settings (1×10^5 for GOLEM and 1.8×10^6 for DAGMA), which yield deterministic runtimes. GOLEM* and DAGMA* consistently outperform their baselines, with F1 improvements of 17.5% and 4.0%, respectively. These gains are attributed to more effective convergence enabled by ALVGL, especially in high-dimensional regimes where baseline methods tend to under-optimize.

ABIC. Fig. 8 shows results for ABIC vs. ABIC* on smaller graphs (15–25 nodes) under linear Gaussian SCMs with latent confounders. We follow the default strategy of selecting the best BIC-scoring graph across five runs. On average, ABIC* improves F1 by 3.1% and reduces runtime

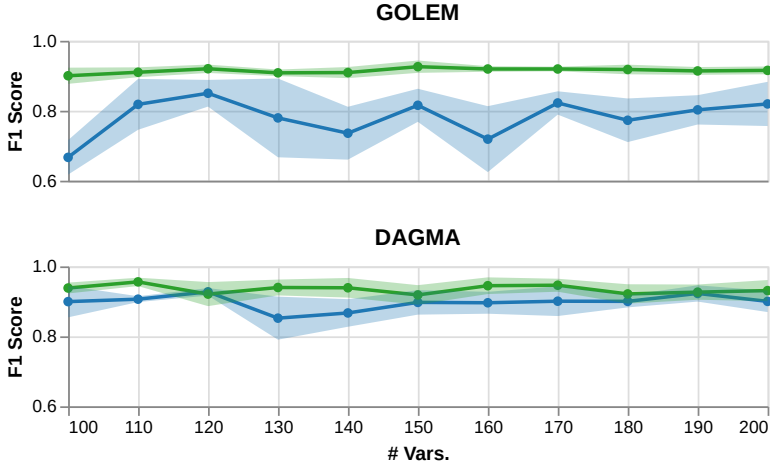


Fig. 7. GOLEM vs. GOLEM* (upper) and DAGMA vs. DAGMA*. (lower)

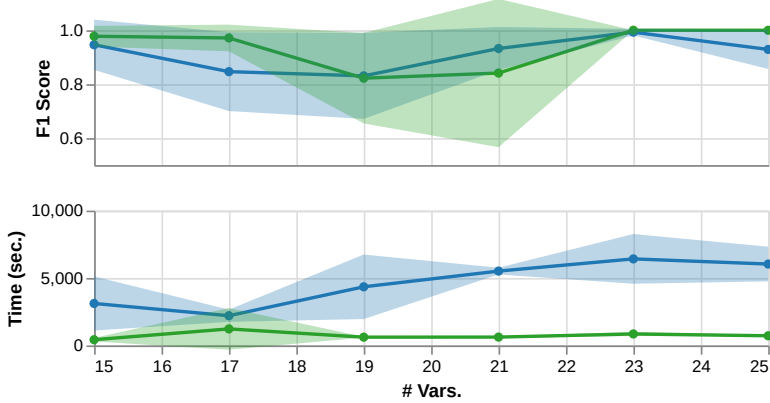


Fig. 8. ABIC vs. ABIC*.

by 77.4%. The runtime gain is particularly significant due to the simplification introduced by super-structure learning in this lower-dimensional setting. One outlier is observed at 21 nodes, where ABIC* underperforms, likely due to instability in optimizing compound graphs under latent confounding.

4.2 Super-Structure Learning Effectiveness

To assess the unique advantages of ALVGL in differentiable causal discovery, we compare it against three alternative super-structure learning approaches applied to NOTEARS:

- **GLasso**: Precision matrix estimation without low-rank modeling, conceptually similar to SDCD [23];
- **LVGL**: ADMM-based latent-variable graphical Lasso [21], omitting our inexact ADMM update and super-structure learning components;
- **SL**: Skeleton-based initialization using the PC algorithm, similar to SPOT [20].

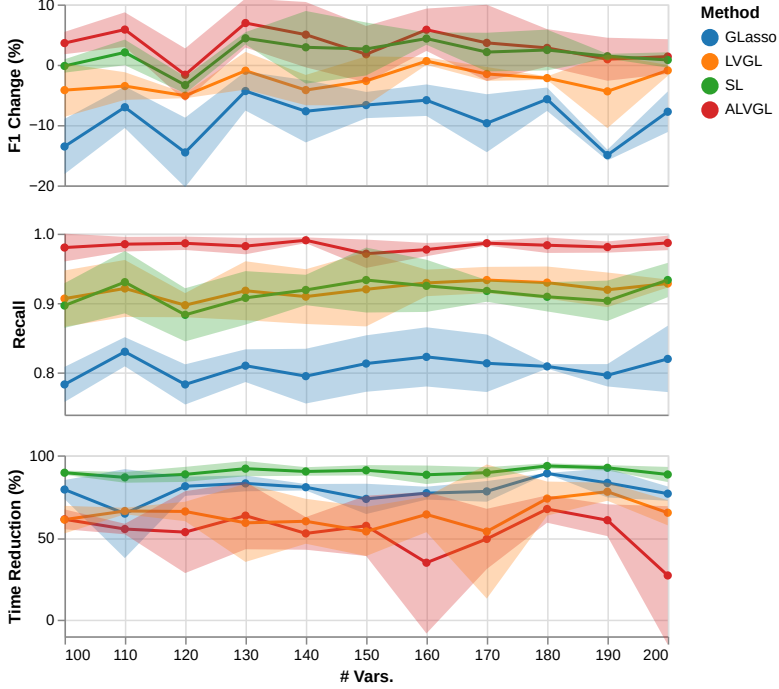


Fig. 9. Comparison of different super-structure learning methods on NOTEARS.

Fig. 9 reports relative changes in F1 score and runtime, along with the average recall of the learned super-structures—crucial for enabling effective downstream optimization. ALVGL achieves the highest F1 improvement (+3.3%), followed by SL (+1.8%), while GLasso and LVGL underperform, primarily due to low super-structure recall. For example, GLasso captures only 0.81 ± 0.016 of true edges, causing irreversible omission during NOTEARS optimization. In contrast, ALVGL achieves a recall of 0.98 ± 0.005 , ensuring most true edges are retained and refined. All methods reduce NOTEARS runtime, with ALVGL achieving a 52.9% speedup despite its larger super-structure. This modest trade-off reflects its broader search space, yet still confirms its efficiency in guiding the optimization.

4.3 Robustness

We evaluate the robustness of ALVGL under varying configurations: graph types, node degrees, sample sizes, and noise distributions. These experiments demonstrate ALVGL’s ability to maintain performance advantages across diverse scenarios while revealing important insights about when and why the method provides greater benefits.

Graph Types. While our main analysis focuses on ER graphs, real-world graphs often follow different topologies, such as SF or BP structures. As shown in Table 2, ALVGL consistently improves F1 scores over vanilla differentiable causal discovery algorithms across all types, with notable gains on BP graphs (12.0% improvement) and demonstrates its ability to capture core causal dependencies even in non-standard structures. The particularly strong performance on BP graphs can be attributed to their more structured sparsity patterns, which align well with ALVGL’s sparse+low-rank decomposition: the bipartite structure naturally induces block-sparse patterns

Table 2. F1 score and runtime (sec.) comparison of NOTEARS with and without ALVGL. The best results are in bold. Varying graph types.

Graph Type	ER	SF	BP
F1 w/o ALVGL	0.928 ± 0.023	0.979 ± 0.011	0.882 ± 0.017
F1 w/ ALVGL	0.948 ± 0.009	0.980 ± 0.009	0.988 ± 0.011
Time w/o ALVGL	349.1 ± 49.5	145.7 ± 45.0	185.6 ± 26.4
Time w/ ALVGL	189.5 ± 12.7	193.9 ± 19.2	173.9 ± 6.6

in the precision matrix that are efficiently captured by the sparse component S , leading to more accurate super-structure learning.

Table 3. F1 score and runtime (sec.) comparison of NOTEARS with and without ALVGL. The best results are in bold. Varying node degree.

Degree	1.00	1.25	1.50	1.75	2.00	2.25	2.50
F1 w/o ALVGL	0.93 ± 0.02	0.95 ± 0.02	0.95 ± 0.02	0.93 ± 0.02	0.96 ± 0.01	0.96 ± 0.01	0.96 ± 0.01
F1 w/ ALVGL	0.95 ± 0.01	0.95 ± 0.01	0.95 ± 0.01	0.95 ± 0.01	0.95 ± 0.01	0.96 ± 0.01	0.95 ± 0.01
Time w/o ALVGL	350 ± 51	758 ± 128	1122 ± 140	1188 ± 183	1731 ± 52	1709 ± 44	1670 ± 282
Time w/ ALVGL	191 ± 13	264 ± 58	472 ± 242	374 ± 121	707 ± 176	838 ± 360	814 ± 151

Node Degree. Table 3 reveals an interesting pattern: ALVGL’s F1 improvement over vanilla algorithms is most pronounced at lower degrees (1.0–1.75), while performance becomes comparable at higher degrees (2.0–2.5). This observation reflects the inherent trade-off in super-structure learning. At lower degrees, the true causal graph is sparser, and ALVGL’s ability to prune the search space from $O(d^2)$ to $O(dk^2)$ (as stated in Corollary 3.3) provides substantial benefits by eliminating spurious edges that would otherwise mislead vanilla algorithms. However, at higher degrees, two competing effects emerge: ① the moralized graph becomes denser, reducing the relative advantage of super-structure pruning, and ② vanilla algorithms themselves perform better on denser graphs as the increased signal strength makes the optimization landscape smoother. Despite this, ALVGL maintains roughly 2×–3× (1.8×–3.2×) runtime improvements across all degree settings, confirming its computational efficiency even when accuracy gains diminish. The runtime benefits warrant further explanation. Even though higher-degree graphs reduce the sparsity advantage, ALVGL’s super-structure initialization provides a better starting point for gradient-based optimization. By constraining the search space (as described in Sec. 3.7), ALVGL prevents the optimizer from exploring large regions of infeasible solutions, leading to faster convergence regardless of the final graph density.

Table 4. F1 score and runtime (sec.) comparison of NOTEARS with and without ALVGL. The best results are in bold. Varying sample size.

<i>n</i>	500	1000	5000	10000
F1 w/o ALVGL	0.925 ± 0.027	0.928 ± 0.023	0.925 ± 0.025	0.929 ± 0.019
F1 w/ ALVGL	0.949 ± 0.003	0.948 ± 0.009	0.965 ± 0.023	0.954 ± 0.035
Time w/o ALVGL	646.1 ± 372.9	377.5 ± 71.7	619.0 ± 268.7	941.8 ± 279.3
Time w/ ALVGL	247.0 ± 107.1	195.3 ± 16.6	572.4 ± 193.8	933.7 ± 45.7

Sample Size. Table 4 shows that F1 improvements remain modest but consistent across all sample sizes, ranging from an absolute increase of 0.024 at $n = 500$ to 0.025 at $n = 10000$ (corresponding to roughly 2.6-2.7% relative improvement over an already high baseline). In contrast, runtime benefits diminish substantially, from a 61.8% reduction at $n = 500$ to only 0.9% at $n = 10000$. This pattern reflects the changing computational bottleneck as sample size increases. At small sample sizes, vanilla algorithms face two challenges: ① high variance in covariance estimation leads to noisy gradients and slower convergence, and ② the search space contains many spurious edges that must be explored and rejected. ALVGL addresses both: its low-rank component L stabilizes the precision matrix estimate (as motivated in Sec. 2.3), and its super-structure pruning eliminates spurious edges a priori. The combination yields substantial speedups (62% faster). However, as n increases, the computational dynamics shift. With more samples, the empirical covariance $\hat{\Sigma}$ becomes well-conditioned, making gradient estimation reliable even in the full $O(d^2)$ search space. vanilla algorithms themselves can now converge efficiently without super-structure guidance where the optimization is no longer bottlenecked by search space size but by the fundamental cost of processing large datasets. Specifically, each gradient computation scales as $O(nd^2 + d^3)$, and at $n = 10000$, this sample size-dependent gradient computation cost dominates any savings from pruning edges. Meanwhile, ALVGL still incurs the overhead of super-structure learning (covariance computation and ADMM), which becomes relatively more expensive as vanilla algorithms' own runtime stabilizes. This explains the vanishing runtime advantage: at $n = 10000$, both methods spend most time computing gradients over large data matrices rather than exploring the graph structure. The ~1% speedup reflects only the marginal benefit of reducing the per-iteration edge count, which is overshadowed by the fixed cost of gradient computation. Having said that, given that many real-world applications operate in small-sample regimes (~100–1000 samples) due to data collection constraints, ALVGL's significant runtime advantages in these settings remain highly relevant and valuable.

Table 5. F1 score and runtime (sec.) comparison of NOTEARS with and without ALVGL. The best results are in bold. Varying noise type.

Noise Type	Gaussian	Exponential	Gumbel	Uniform
F1 w/o ALVGL	0.928 ± 0.023	0.925 ± 0.016	0.914 ± 0.023	0.840 ± 0.017
F1 w/ ALVGL	0.948 ± 0.009	0.914 ± 0.018	0.904 ± 0.043	0.902 ± 0.032
Time w/o ALVGL	351.5 ± 41.5	455.2 ± 151.4	526.3 ± 127.5	298.6 ± 177.9
Time w/ ALVGL	189.4 ± 16.0	257.4 ± 53.1	210.0 ± 25.1	180.2 ± 17.2

Non-Gaussian Noise. Although ALVGL is grounded in linear Gaussian assumptions, we test its robustness on data with exponential, Gumbel, and uniform noise (see Table 5). Results show graceful degradation: F1 scores remain competitive under exponential noise (with slight degradation) and improve substantially under uniform noise (from 0.84 to 0.90). The varying performance can be explained by the degree of distributional mismatch. Exponential and Gumbel distributions are asymmetric and heavy-tailed, violating Gaussianity more severely and potentially introducing bias in the precision matrix estimate. In contrast, uniform noise, while non-Gaussian, is symmetric and bounded, leading to less severe misspecification. Under uniform noise, ALVGL's low-rank component effectively captures deviations from Gaussianity as latent structure, inadvertently improving robustness. Importantly, ALVGL retains substantial runtime benefits across all noise types (about 40-60% reduction), which suggests strong practical robustness to distributional misspecification. We presume this is because the super-structure learning step primarily relies on correlation patterns rather than exact distributional assumptions, allowing it to guide optimization effectively even

when the Gaussian assumption is violated. NOTEARS with or without ALVGL fails under logistic and Poisson noise due to optimization instability and are excluded from this analysis; exploring discrete and non-linear extensions remains future work.

Summary. These robustness experiments reveal that ALVGL provides the greatest accuracy improvements when: ① graphs are sparse (low degree), ② sample sizes are limited, and ③ noise distributions are Gaussian or moderately non-Gaussian but symmetric. However, computational benefits persist across all settings, making ALVGL a universally beneficial enhancement for differentiable causal discovery pipelines, particularly in high-dimensional regimes where optimization efficiency is critical.

4.4 Real-world Data

Table 6. Precision, recall and F1 score on Sachs dataset. The best results are in bold.

Methods	NOTEARS*	NOTEARS w/ GLasso	NOTEARS w/ LVGL	NOTEARS
Precision	0.67	0.63	0.71	0.57
Recall	0.32	0.26	0.26	0.21
F1-Score	0.43	0.37	0.38	0.31

We evaluate ALVGL on the Sachs dataset [29], which contains 7466 cells ($n = 7466$) and flow cytometry measurements of 11 ($d = 11$) phosphorylated proteins and phospholipids. The F1 score is computed against the consensus CPDAG ground truth. As shown in Table 6, NOTEARS* achieves the highest F1 score of 0.43, significantly outperforming the baseline NOTEARS score of 0.31.

In this setting ($n \gg d$), while covariance estimation is stable, the primary challenge stems from complex biological dependencies that are not fully captured by the strict linear Gaussian assumptions of the model. This misspecification creates a difficult optimization landscape, leading baseline NOTEARS to miss a large proportion of true causal edges, resulting in a poor recall of 0.21. The key advantage of ALVGL lies in providing a reliable estimation of the super-structure to guide the search. By identifying a comprehensive set of plausible edges that capture both direct signals and associations potentially obscured by confounding, it enables NOTEARS to focus its optimization on the variable pairs that matter most in the underlying graph. This targeted search leads to a substantial improvement in recall to 0.32 and the best overall F1 score.

Comparing the alternatives highlights the effectiveness of ALVGL’s specific design. NOTEARS w/ GLasso ignores potential latent structures, yielding only partial improvement. NOTEARS w/ LVGL employs a standard decomposition that appears too conservative for this task; while it achieves high precision (0.71), its low recall (0.26) suggests it prematurely prunes true edges from the search space. NOTEARS*, by explicitly combining sparse and low-rank evidence into the super-structure, strikes the best balance, maximizing recall among super-structure methods and enabling the downstream optimizer to reconstruct the most accurate graph.

Unlike our synthetic benchmarks, Sachs data does not strictly satisfy linear Gaussian assumptions. The observed improvement here is complementary to findings in Sec. 4.3, demonstrating ALVGL’s practical robustness. Even in low-dimensional, large-sample real-world scenarios, its approach to reliably constraining the search space provides a critical advantage over unstructured optimization, leading to more accurate causal discovery.

5 Related Work

Differentiable Causal Discovery. Differentiable methods have recently emerged as a promising approach for improving the accuracy and efficiency of causal discovery. These methods reformulate the problem as a continuous optimization task, enabling the use of gradient-based algorithms to learn causal structures directly from data. Notable examples include NOTEARS [41], GOLEM [24], DAGMA [3], and ABIC [4]. Subsequent work has focused on enhancing performance through various means: improving the stability and computational efficiency of acyclicity constraints [3, 34, 36, 40, 42]; incorporating domain knowledge and interventional data [2, 6, 13, 16]; extending expressiveness to handle more complex functional forms [1, 15, 19]; and increasing robustness to model misspecification [35, 37]. In this paper, we contribute a novel yet complementary enhancement by introducing a reliable super-structure learning step into the optimization pipeline, which significantly improves optimization efficiency.

Structure Learning. Structure learning is a central task in probabilistic graphical models (PGMs), where the goal is to uncover the underlying conditional independence structure among variables. Classical approaches typically focus on learning structures such as Markov blankets [17], conditional independence graphs [22], or full network structures [26], using score-based, constraint-based, or hybrid algorithms. In high-dimensional settings, sparsity assumptions and regularization techniques such as graphical Lasso [14] have been widely adopted to ensure statistical and computational tractability. While much of this literature focuses on identifying precise conditional dependencies, we instead aim to learn a coarser but reliable super-structure that guides downstream differentiable optimization. Despite its simplicity, our approach outperforms existing methods targeting exact structures on downstream tasks.

6 Conclusion

In this paper, we introduced ALVGL, a novel and general enhancement to the differentiable causal discovery pipeline. By learning a super-structure that captures the core causal dependencies, ALVGL significantly reduces the search space and improves optimization efficiency. We demonstrated the versatility of ALVGL across various structural causal models, including Gaussian and non-Gaussian settings, with and without unmeasured confounders. Extensive experiments on synthetic and real-world datasets showed that ALVGL not only achieves state-of-the-art accuracy but also significantly improves optimization efficiency, making it a reliable and efficient solution for differentiable causal discovery.

References

- [1] Matthew Ashman, Chao Ma, Agrin Hilmkil, Joel Jennings, and Cheng Zhang. 2022. Causal Reasoning in the Presence of Latent Confounders via Neural ADMG Learning. In *The Eleventh International Conference on Learning Representations*.
- [2] Taiyu Ban, Lyuzhou Chen, Xiangyu Wang, Xin Wang, Derui Lyu, and Huanhuan Chen. 2024. Differentiable structure learning with partial orders. *Advances in Neural Information Processing Systems* 37 (2024), 117426–117455.
- [3] Kevin Bello, Bryon Aragam, and Pradeep Ravikumar. 2022. Dagma: Learning dags via m-matrices and a log-determinant acyclicity characterization. *Advances in Neural Information Processing Systems* 35 (2022), 8226–8239.
- [4] Rohit Bhattacharya, Tushar Nagarajan, Daniel Malinsky, and Ilya Shpitser. 2021. Differentiable causal discovery under unmeasured confounding. In *International Conference on Artificial Intelligence and Statistics*. PMLR, 2314–2322.
- [5] Stephen Boyd, Neal Parikh, Eric Chu, Borja Peleato, Jonathan Eckstein, et al. 2011. Distributed optimization and statistical learning via the alternating direction method of multipliers. *Foundations and Trends® in Machine learning* 3, 1 (2011), 1–122.
- [6] Philippe Brouillard, Sébastien Lachapelle, Alexandre Lacoste, Simon Lacoste-Julien, and Alexandre Drouin. 2020. Differentiable causal discovery from interventional data. *Advances in Neural Information Processing Systems* 33 (2020), 21865–21877.
- [7] Peter Bühlmann, Jonas Peters, and Jan Ernest. 2014. CAM: Causal additive models, high-dimensional order search and penalized regression. *Annals of Stats.* (2014).

- [8] Venkat Chandrasekaran, Pablo A Parrilo, and Alan S Willsky. 2012. Latent variable graphical model selection via convex optimization. *The Annals of Statistics* (2012), 1935–1967.
- [9] Rui Chen, Sanjeeb Dash, and Tian Gao. 2021. Integer programming for causal structure learning in the presence of latent variables. In *International Conference on Machine Learning*. PMLR, 1550–1560.
- [10] Tom Claassen and Ioan G Bucur. 2022. Greedy equivalence search in the presence of latent confounders. In *Uncertainty in Artificial Intelligence*. PMLR, 443–452.
- [11] Diego Colombo, Marloes H Maathuis, Markus Kalisch, and Thomas S Richardson. 2012. Learning high-dimensional directed acyclic graphs with latent and selection variables. *Annals of Stats.* (2012).
- [12] Jonathan Eckstein and Dimitri P Bertsekas. 1992. On the Douglas–Rachford splitting method and the proximal point algorithm for maximal monotone operators. *Mathematical programming* 55 (1992), 293–318.
- [13] Gonçalo Rui Alves Faria, Andre Martins, and Mário AT Figueiredo. 2022. Differentiable causal discovery under latent interventions. In *Conference on Causal Learning and Reasoning*. PMLR, 253–274.
- [14] Jerome Friedman, Trevor Hastie, and Robert Tibshirani. 2008. Sparse inverse covariance estimation with the graphical lasso. *Biostatistics* 9, 3 (2008), 432–441.
- [15] Tomas Geffner, Javier Antoran, Adam Foster, Wenbo Gong, Chao Ma, Emre Kiciman, Amit Sharma, Angus Lamb, Martin Kukla, Agrin Hilmkil, et al. 2022. Deep End-to-end Causal Inference. In *NeurIPS 2022 Workshop on Causality for Real-world Impact*.
- [16] Adam Li, Amin Jaber, and Elias Bareinboim. 2023. Causal discovery from observational and interventional data across multiple environments. *Advances in Neural Information Processing Systems* 36 (2023), 16942–16956.
- [17] Zhaolong Ling, Kui Yu, Hao Wang, Lin Liu, Wei Ding, and Xindong Wu. 2019. BAMB: A balanced Markov blanket discovery approach to feature selection. *ACM Transactions on Intelligent Systems and Technology (TIST)* 10, 5 (2019), 1–25.
- [18] Po-Ling Loh and Peter Bühlmann. 2014. High-dimensional learning of linear causal networks via inverse covariance estimation. *Journal of Machine Learning Research* 15, 140 (2014), 3065–3105.
- [19] Lars Lorch, Jonas Rothfuss, Bernhard Schölkopf, and Andreas Krause. 2021. Dibs: Differentiable bayesian structure learning. *Advances in Neural Information Processing Systems* 34 (2021), 24111–24123.
- [20] Pingchuan Ma, Rui Ding, Qiang Fu, Jiaru Zhang, Shuai Wang, Shi Han, and Dongmei Zhang. 2024. Scalable Differentiable Causal Discovery in the Presence of Latent Confounders with Skeleton Posterior. In *Proceedings of the 30th ACM SIGKDD Conference on Knowledge Discovery and Data Mining*. 2141–2152.
- [21] Shiqian Ma, Lingzhou Xue, and Hui Zou. 2013. Alternating direction methods for latent variable Gaussian graphical model selection. *Neural computation* 25, 8 (2013), 2172–2198.
- [22] NICOLAI MEINSHAUSEN and PETER BÜHLMANN. 2006. HIGH-DIMENSIONAL GRAPHS AND VARIABLE SELECTION WITH THE LASSO. *The Annals of Statistics* 34, 3 (2006), 1436–1462.
- [23] Achille Nazaret, Justin Hong, Elham Azizi, and David Blei. 2024. Stable differentiable causal discovery. In *Proceedings of the 41st International Conference on Machine Learning*. 37413–37445.
- [24] Ignavier Ng, AmirEmad Ghassami, and Kun Zhang. 2020. On the role of sparsity and dag constraints for learning linear dags. *Advances in Neural Information Processing Systems* 33 (2020), 17943–17954.
- [25] Ignavier Ng, Yujia Zheng, Jiji Zhang, and Kun Zhang. 2021. Reliable causal discovery with improved exact search and weaker assumptions. *Advances in Neural Information Processing Systems* 34 (2021), 20308–20320.
- [26] Jonas Peters, Dominik Janzing, and Bernhard Schölkopf. 2017. *Elements of causal inference*. The MIT Press.
- [27] Thomas Richardson and Peter Spirtes. 2002. Ancestral graph Markov models. *The Annals of Statistics* 30, 4 (2002), 962–1030.
- [28] Raanan Y Rohekar, Shami Nisimov, Yaniv Gurwicz, and Gal Novik. 2021. Iterative causal discovery in the possible presence of latent confounders and selection bias. *Advances in Neural Information Processing Systems* 34 (2021), 2454–2465.
- [29] Karen Sachs, Omar Perez, Dana Pe'er, Douglas A Lauffenburger, and Garry P Nolan. 2005. Causal protein-signaling networks derived from multiparameter single-cell data. *Science* (2005).
- [30] Peter Spirtes, Clark N Glymour, Richard Scheines, and David Heckerman. 2000. *Causation, prediction, and search*. MIT press.
- [31] Ioannis Tsamardinos, Laura E Brown, and Constantin F Aliferis. 2006. The max-min hill-climbing Bayesian network structure learning algorithm. *Machine learning* 65 (2006), 31–78.
- [32] Konstantinos Tsirlis, Vincenzo Lagani, Sofia Triantafillou, and Ioannis Tsamardinos. 2018. On scoring maximal ancestral graphs with the max–min hill climbing algorithm. *International Journal of Approximate Reasoning* 102 (2018), 74–85.
- [33] Matthew J Vowels, Necati Cihan Camgoz, and Richard Bowden. 2022. D'ya like dags? a survey on structure learning and causal discovery. *Comput. Surveys* 55, 4 (2022), 1–36.
- [34] Dennis Wei, Tian Gao, and Yue Yu. 2020. DAGs with No Fears: A closer look at continuous optimization for learning Bayesian networks. *Advances in Neural Information Processing Systems* 33 (2020), 3895–3906.

- [35] Huiyang Yi, Yanyan He, Duxin Chen, Mingyu Kang, He Wang, and Wenwu Yu. 2025. The Robustness of Differentiable Causal Discovery in Misspecified Scenarios. In *The Thirteenth International Conference on Learning Representations*.
- [36] Yue Yu, Jie Chen, Tian Gao, and Mo Yu. 2019. DAG-GNN: DAG structure learning with graph neural networks. In *International conference on machine learning*. PMLR, 7154–7163.
- [37] An Zhang, Fangfu Liu, Wenchang Ma, Zhibo Cai, Xiang Wang, and Tat-Seng Chua. 2023. Boosting Causal Discovery via Adaptive Sample Reweighting. In *The Eleventh International Conference on Learning Representations*.
- [38] Jiji Zhang. 2008. On the completeness of orientation rules for causal discovery in the presence of latent confounders and selection bias. *Artificial Intelligence* 172, 16–17 (2008), 1873–1896.
- [39] Zhen Zhang, Ignavier Ng, Dong Gong, Yuhang Liu, Ehsan Abbasnejad, Mingming Gong, Kun Zhang, and Javen Qinfeng Shi. 2022. Truncated matrix power iteration for differentiable DAG learning. *Advances in Neural Information Processing Systems* 35 (2022), 18390–18402.
- [40] Zhen Zhang, Ignavier Ng, Dong Gong, Yuhang Liu, Mingming Gong, Biwei Huang, Kun Zhang, Anton van den Hengel, and Javen Qinfeng Shi. 2025. Analytic DAG Constraints for Differentiable DAG Learning. *arXiv preprint arXiv:2503.19218* (2025).
- [41] Xun Zheng, Bryon Aragam, Pradeep K Ravikumar, and Eric P Xing. 2018. Dags with no tears: Continuous optimization for structure learning. *Advances in neural information processing systems* 31 (2018).
- [42] Xun Zheng, Chen Dan, Bryon Aragam, Pradeep Ravikumar, and Eric Xing. 2020. Learning sparse nonparametric dags. In *International Conference on Artificial Intelligence and Statistics*. Pmlr, 3414–3425.